Supplementary Information:

Rapid Electron/Ion Transport in a 3D Holey-Graphene Aerogel Framework toward High-Loading Na–Se Batteries

Ningxun Zhang, Zheng Yang, Chenyang Gao, Xu Tan, Wenlu Yuan, Tao Wang,* Yuping Wu*

Confucius Energy Storage Lab, Z Energy Storage Center & School of Energy and Environment, Southeast University, Nanjing 211189, P. R. China

E-mail: wangtao2021@seu.edu.cn; wuyp@seu.edu.cn

Experimental Procedures

Materials

Polyacrylonitrile (PAN, M_w = 150000), selenium powder (Se), N-methyl-2-pyrrolidone (NMP) and sodium ascorbate (SA) were obtained from Shanghai Aladdin Biochemical Technology Co., Ltd. Ketjen black and polyvinylidene difluoride (PVDF) were obtained from Canrd Co., Ltd. The graphene oxide (GO) dispersion was obtained from GaoxiTech Co., Ltd. Multi-walled carbon nanotubes (MWCNTs) were obtained from Shenzhen Suiheng Technology Co., Ltd. Ethylene carbonate (EC), diethyl carbonate (DEC), 1,2-dimethoxyethane (DME), tetraethylene glycol dimethyl ether (TETRAGLYME) and sodium hexafluorophosphate ($NaPF_6$) were obtained from Suzhou DoDochem Co., Ltd., China. All materials were used without further purification.

Synthesis of the SePAN Powder

PAN and Se powder (mass ratio 1:1.5) were homogeneously mixed and subsequently annealed at 500 °C for 6 h under argon (Ar) atmosphere with a heating rate of 2 °C min^{-1}. After naturally cooling to room temperature, a black SePAN powder was obtained.

Synthesis of the HGO

A total of 5 mL of 30% H_2O_2 aqueous solution was added to 50 mL of GO dispersion (2 mg mL^{-1}) and heated at 100 °C with continuous stirring for 2 h. The obtained HGO was purified by centrifugation and washing to remove residual H_2O_2, and then redispersed in deionized water to achieve a concentration of 1 mg mL^{-1}.

Synthesis of the SePAN@3DHG Composite

SePAN powder (25 mg) was uniformly dispersed in 5 mL of HGO dispersion (1 mg mL^{-1}), followed by the addition of 30 mg sodium ascorbate (SA), which facilitates the reduction and self-assembly of graphene oxide. The mixture was magnetically stirred to obtain a homogeneous suspension. Subsequently, 0.2−1.5 mL of the mixture was transferred into glass vials with a diameter of 10 mm and heated at 95 °C for 6 h in a sealed container to obtain SePAN@3DHG hydrogel composites. The obtained

materials were repeatedly washed with deionized water to eliminate residual impurities. After freeze-drying, the samples were annealed at 500 °C for 3 h under an Ar flow to further enhance the conductivity of graphene. SePAN@3DG was synthesized following the same procedure, except that pristine GO dispersion without etching treatment was used.

Preparation of the SePAN-coated Cathode

80 wt% SePAN powder, 10 wt% Ketjen black, and 10 wt% PVDF were dispersed in NMP to form a uniform slurry, which was then coated onto Al foil and dried in a vacuum oven at 60 °C overnight. The electrodes were punched into discs with 10 mm in diameter.

Synthesis of the Se/CNT Composite

The Se/CNT composite was prepared *via* a melt-diffusion method. Se powder and multi-walled carbon nanotubes (MWCNTs) were uniformly mixed at a mass ratio of 7:3, and the mixture was annealed at 260 °C for 12 h in a tube furnace under an Ar atmosphere with a heating rate of 5 °C min^{-1}. After naturally cooling to room temperature, a black Se/CNT composite was obtained.

Materials Characterization

Scanning electron microscopy (SEM) images and energy-dispersive X-ray (EDX) spectroscopy mappings were captured using a ZEISS Sigma 300 microscope. The energy-dispersive spectrometer model employed for the analysis was the Oxford Xplore 50. The transmission electron microscopy (TEM) images were obtained from a field emission transmission electron microscope (FE-TEM, Tecnai F20). Specific surface area and pore size distribution of the sample were measured by Brunauer-Emmett-Teller (BET) N_2 adsorption-desorption and density functional theory analysis method (ASAP 2020, Micromeritics). The thermal gravimetric analyzer (TGA) testing was performed with a temperature range from 25 to 850 °C in N_2 atmosphere at a heating rate of 10 °C min^{-1} (HENVEN HTG-1). Elemental analysis (EA) was conducted by Elementar-UNICUBE. X-ray diffraction (XRD) patterns were recorded by Rigaku X-ray diffractometer with Cu Kα radiation from 10° to 60° at a sweep rate of 6° min^{-1}. Fourier transform infrared (FT-IR) spectra were collected by the Bruker

ALPHA spectrometer with ATR. Raman spectra were performed using a confocal Raman system (WITec Alpha 300 Access). UV-vis spectra were recorded using a spectrophotometer (Varian Cary 50 Conc). X-ray photoelectron spectroscopy (XPS) was conducted by Thermo Scientific K-Alpha spectrometer.

Electrochemical Measurements

The electrochemical tests were performed *via* assembling CR2032-type coin cells in an Ar-filled glove box. 1 M $NaPF_6$ in EC and DEC (*v*:*v*=1:1) was used as the electrolyte. The E/S ratio was tuned as the SePAN loading increased, decreasing from 20 (≤ 5 mg cm^{-2}) to 10 (5–10 mg cm^{-2}) and 8 (> 10 mg cm^{-2}). Glass fiber separator (Whatman GF/D) was used. The circular sodium foil with a diameter of 14 mm was used as the anode. The galvanostatic discharge/charge measurements and GITT curves were performed using a Neware battery test system. The specific capacity was calculated based on the mass of selenium. CV curves and *in-situ* EIS measurements were performed by the electrochemical workstation (Bio-logic, VMP-300). EIS measurements were performed in the frequency range from 100 kHz to 0.01 Hz.

Fabrication of Stainless-Steel Symmetric Cells

The blank graphene aerogel without SePAN powder (3DHG/3DG) was crushed into powder and uniformly mixed with PVDF at a mass ratio of 9:1. The mixture was added to NMP and stirred to obtain a uniform slurry. Subsequently, the slurry was coated onto a Celgard 2500 separator and dried overnight at 40 °C to obtain HG/PP and G/PP. For the symmetric configuration, stainless steel disks with a diameter of 16 mm were used as both electrodes, while a 19 mm HG/PP or G/PP separator was placed between them.

Supplementary Figures:

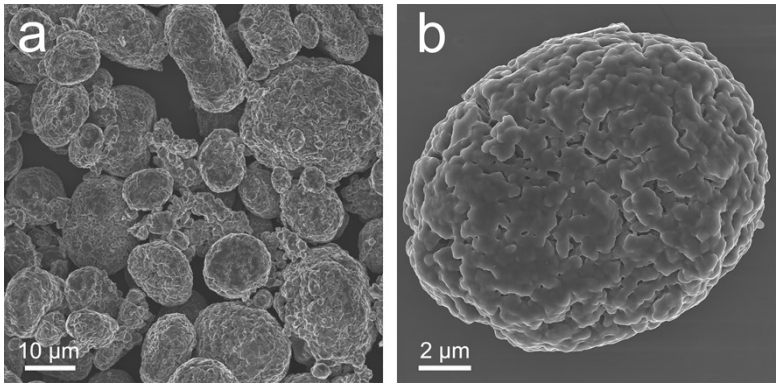

Fig. S1 SEM images of SePAN powder.

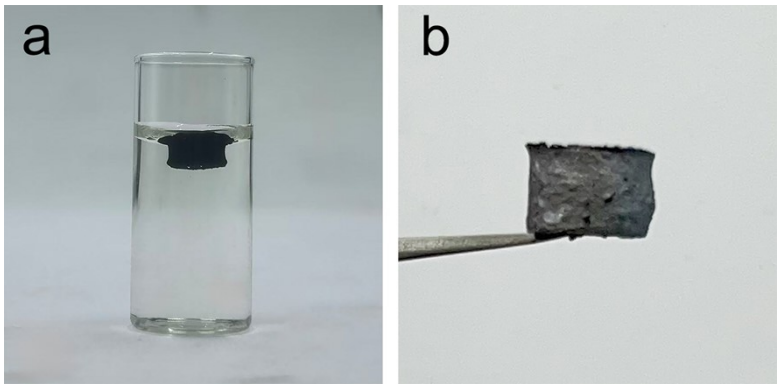

Fig. S2 Digital images of (a) the hydrothermally prepared SePAN@3DHG hydrogel and (b) the aerogel after freeze-drying and annealing.

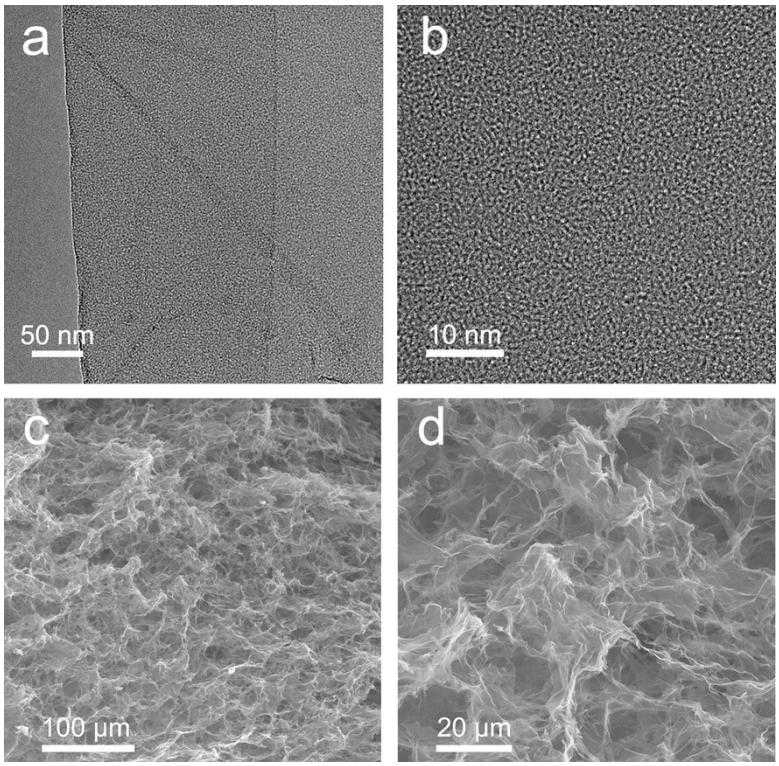

Fig. S3 (a,b) Typical TEM images of GO sheets. (c,d) SEM images of 3DHG.

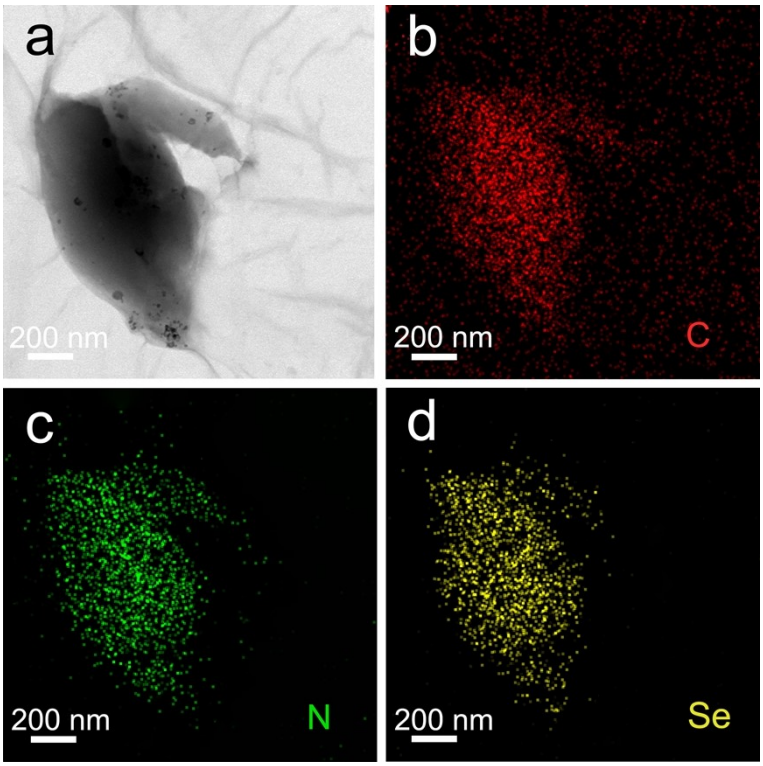

Fig. S4 TEM-EDS mapping images of SePAN@3DHG.

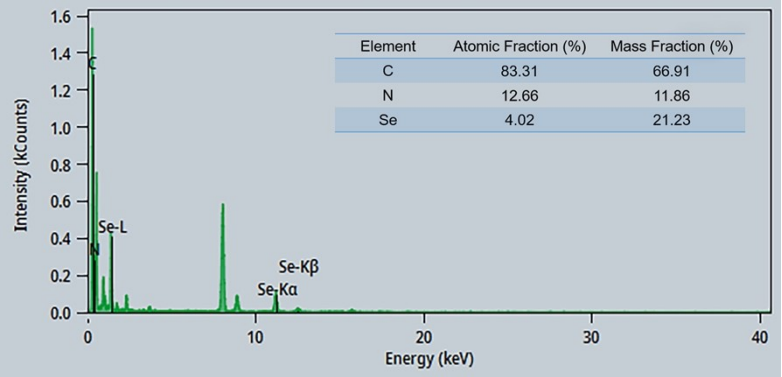

Fig. S5 TEM-EDS spectrum of SePAN@3DHG.

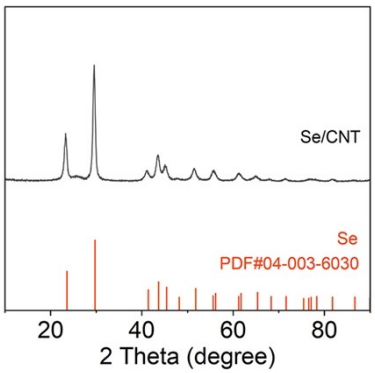

Fig. S6 XRD pattern of Se/CNT composite.

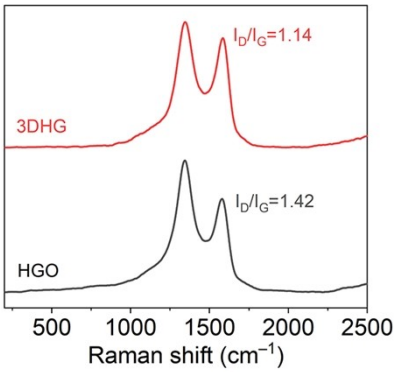

Fig. S7 Raman spectra of HGO and 3DHG.

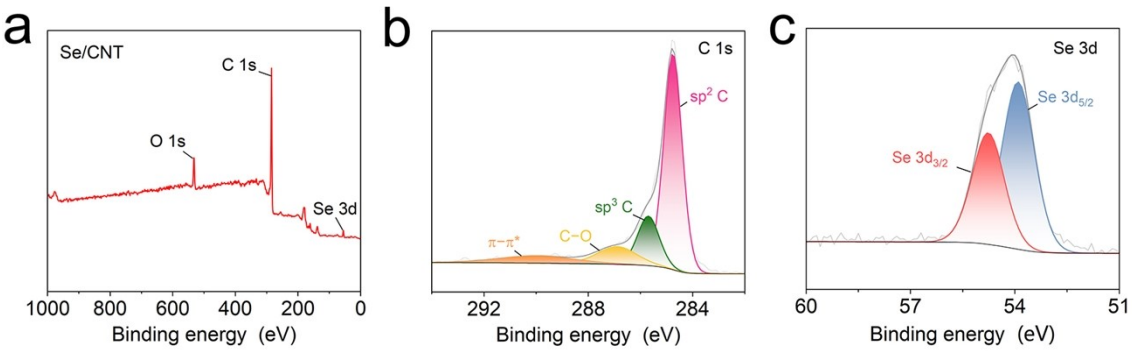

Fig. S8 (a)XPS survey spectrum of Se/CNT composite and high-resolution XPS spectra of (b) C 1s, (c) Se 3d.

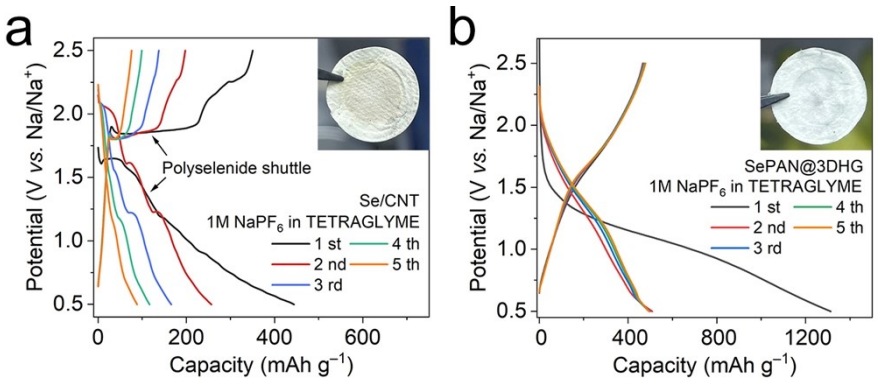

Fig. S9 Charge–discharge curves of (a) Se/CNT and (b) SePAN@3DHG electrodes in ether-based electrolyte (inset: digital photographs of the corresponding separators after cycling).

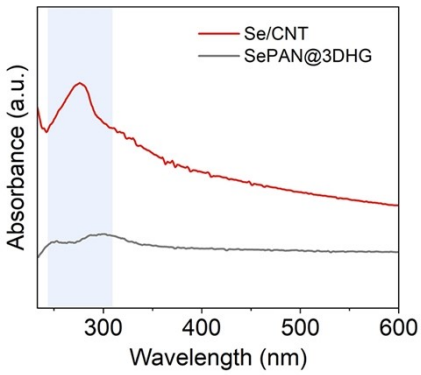

Fig. S10 UV-vis absorption spectra of the DME washing solutions from Se/CNT and SePAN@3DHG cells after cycling.

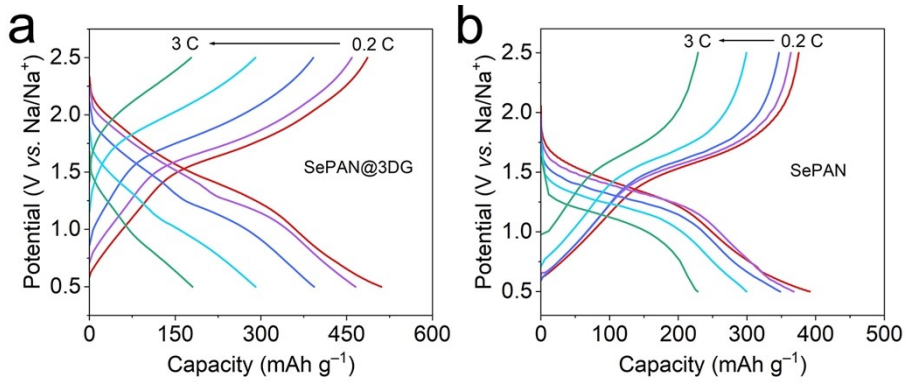

Fig. S11 Charge–discharge curves of (a) SePAN@3DG, (b) SePAN at different current rates.

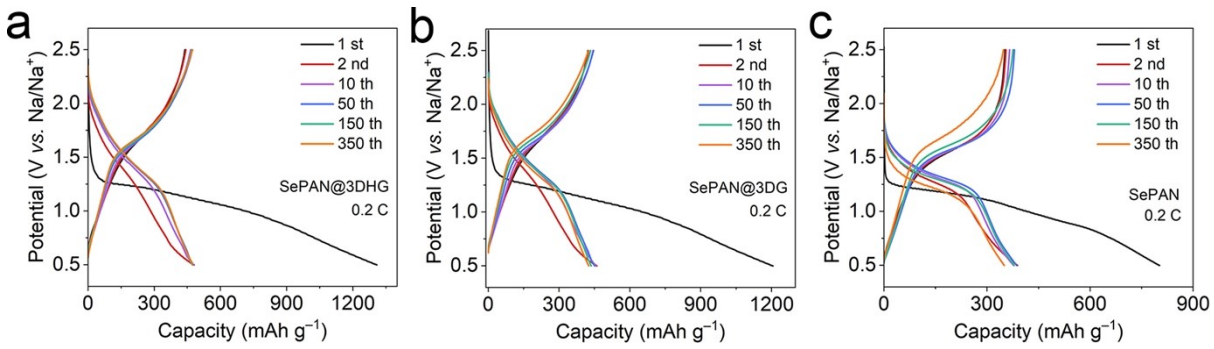

Fig. S12 Charge–discharge curves of (a) SePAN@3DHG, (b) SePAN@3DG and (c) SePAN at 0.2 C.

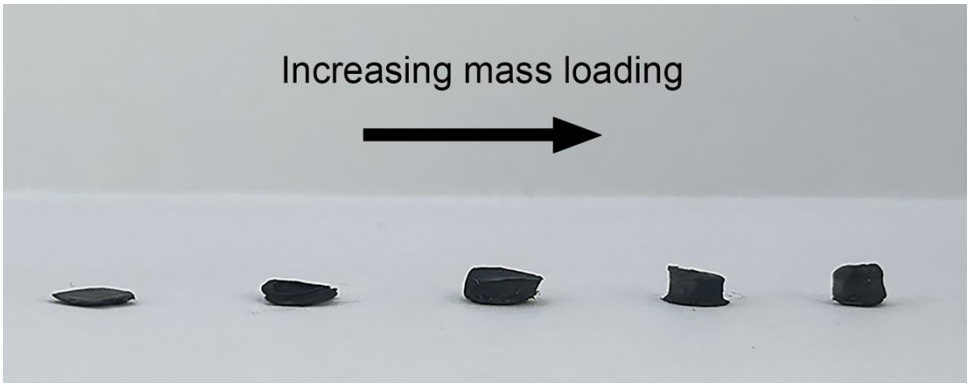

Fig. S13 Digital photograph of SePAN@3DHG electrodes with gradient mass loadings.

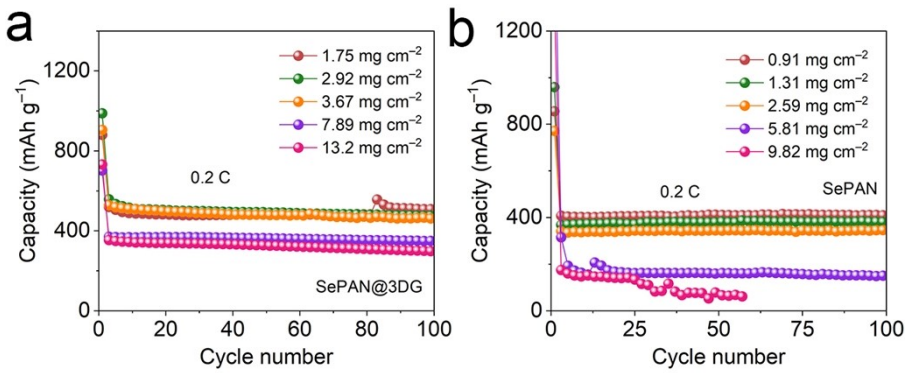

Fig. S14 Cycling performance of (a) SePAN@3DG and (b) SePAN electrodes at 0.2 C under different mass loadings.

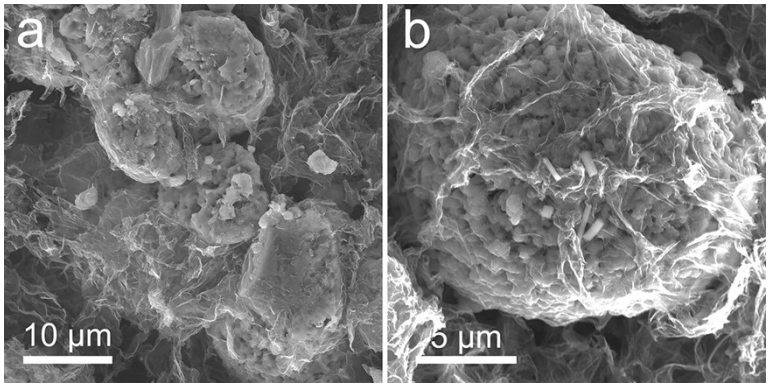

Fig. S15 SEM images of the SePAN@3DHG electrode after cycling.

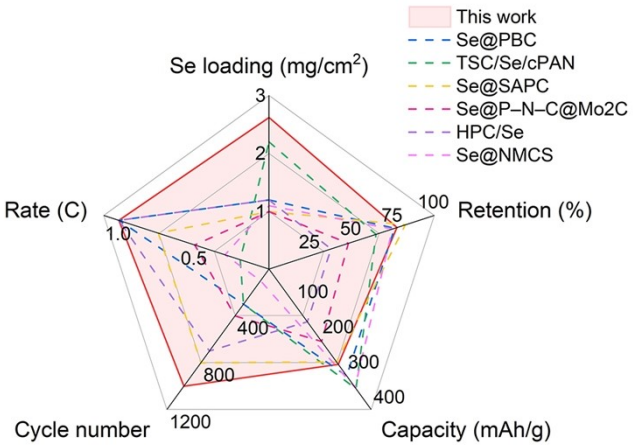

Fig. S16 Electrochemical performance comparison between SePAN@3DHG and recently reported Se/C composite cathodes for Na–Se batteries.[1-6]

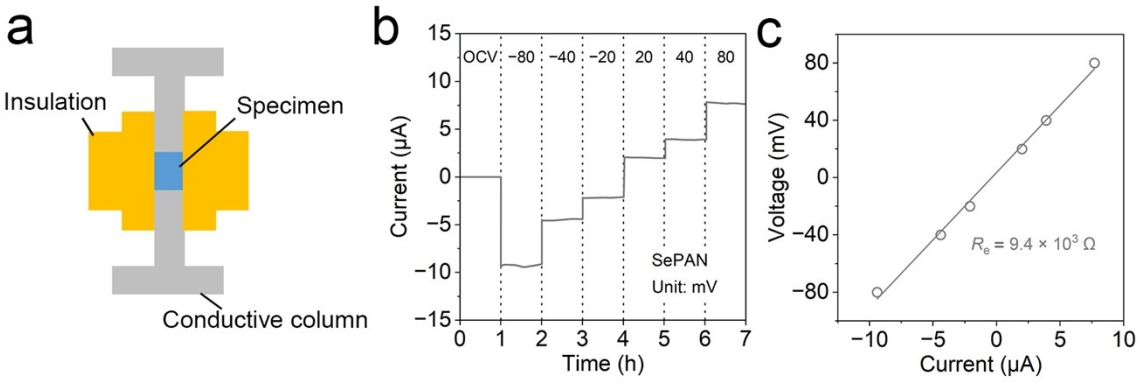

Fig. S17 (a) Schematic illustration of the DC polarization measurements configuration. (b,c) Electronic resistance of SePAN measured by DC polarization.[7, 8]

*DC polarization measurements were conducted using a custom-built setup (Fig. S17a), in which the sample was sandwiched between two stainless-steel electrodes within an insulating casing. A pressure of 1000 psi was applied prior to measurement and maintained by bolts (8.4–8.5 N·m) to ensure good interfacial contact. A stepwise voltage protocol was employed, with each step held for 1 h and a 5 s interval between steps, while the current response was continuously recorded.

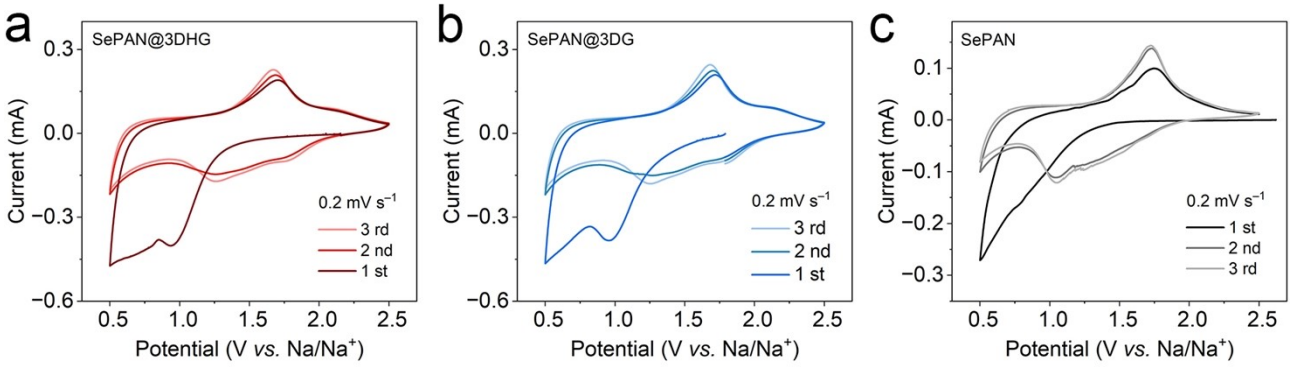

Fig. S18 The initial 3 cycles CV curves of (a) SePAN@3DHG, (b) SePAN@3DG and (c) SePAN.

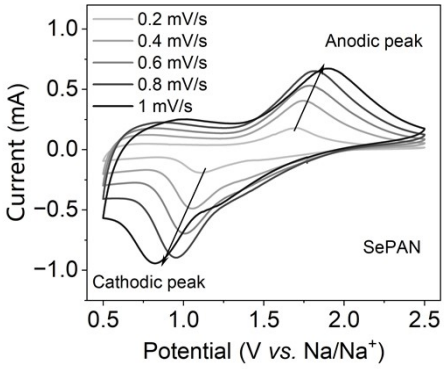

Fig. S19 CV curves of SePAN with different scanning rates.

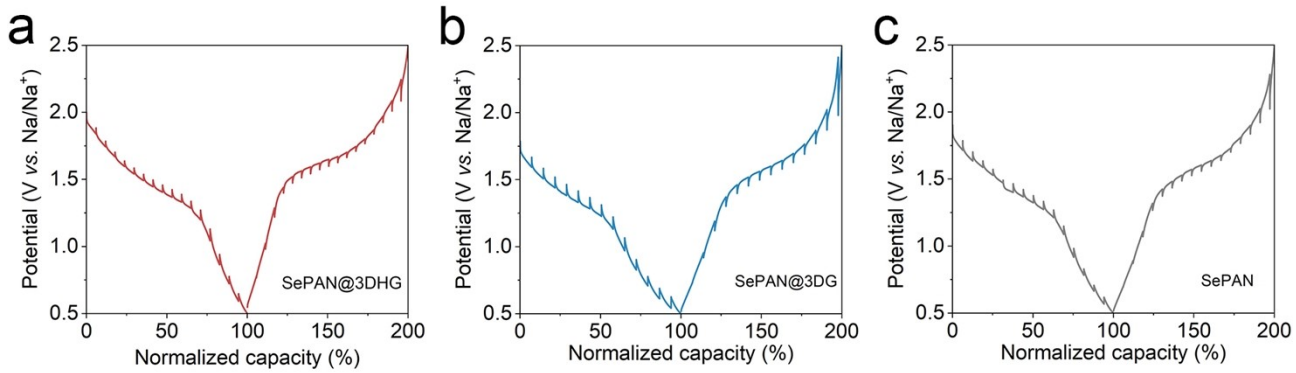

Fig. S20 GITT curves of (a) SePAN@3DHG, (b) SePAN@3DG and (c) SePAN.

* The GITT test was conducted by discharging or charging batteries at a current density of 0.1 C for 30 minutes, followed by a resting period of 2 h. The Na^+ diffusion coefficient (D_{Na+}) derived from GITT was calculated using the following equation:[9,10]

$$D_{Na+} = \frac{4}{\pi\tau}\left(\frac{m_B V_M}{M_B S}\right)^2\left(\frac{\Delta E_S}{\Delta E_\tau}\right)^2 \qquad Eq.S1$$

where τ is the duration of the current impulse, m_B is the mass loading of the active material, S represents the electrode area, ΔE_S is the quasi-thermodynamic equilibrium potential difference between before and after the current pulse, ΔE_τ represents the potential difference during the current pulse; V_M is the molar volume of the active material, and M_B is the molar mass of active material.

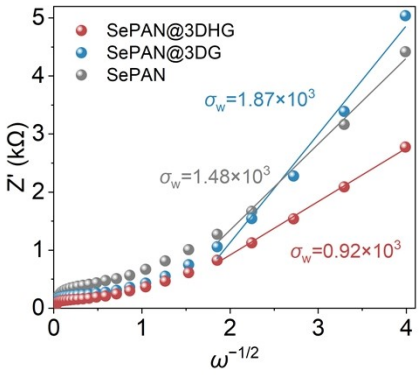

Fig. S21 Linear fitting of the Z'-$\omega^{-1/2}$ plots and the corresponding Warburg coefficient determination for SePAN@3DHG, SePAN@3DG, and SePAN. (Z' represents the real part of the impedance; $\omega=2\pi f$ denotes the angular frequency).[11]

Supplementary Tables:

Table S1 Elemental analysis of SePAN@3DHG and SePAN.

Sample	C (wt%)	N (wt%)	H (wt%)	Se (wt%)
SePAN@3DHG	52.35	10.32	1.713	35.62
SePAN	43.85	12.11	1.216	42.82

***Determination of Se loading based on TGA.** CPAN was directly obtained through the carbonization of PAN. In the test temperature range, the weight loss of CPAN is 18.52%. Therefore, the 44.78% weight loss of SePAN@3DHG is caused by the loss of Se and the reduction of CPAN weight. Suppose the content of Se in SePAN@3DHG is X and the content of CPAN is Y. The relationship between them is as follows:[12]

$$X + Y = 100\%$$

$$X + Y \times 18.52\% = 44.78\%$$

According to the relationship, the content of Se in SePAN@3DHG can be calculated, which is X = 32.2%. Using the same relationship, the Se content of SePAN was determined to be 44.0%. The Se content determined by elemental analysis (35.6 wt%) is slightly higher than that calculated from TGA (32.2 wt%), which may arise from different measurement principles.-The EA result was adopted in the main text because EA provides quantitative analysis, whereas TGA in this case is more suitable for qualitative support than precise quantification.

Table S2 Electronic conductivity calculation of SePAN@3DHG, SePAN/CB, and SePAN.

Specimen	R_e (Ω)	A (cm^2)	d (μm)	σ_e (S cm^{-1})
SePAN@3DHG	0.24	0.785	250	1.33×10^{-1}
SePAN/CB	0.36	0.785	290	1.03×10^{-1}
SePAN	9.4×10^{3}	0.785	220	2.98×10^{-6}

*The electronic conductivity (σ_e) of the specimen was calculated using the following equation:[7]

$$\sigma_e = \frac{d}{AR_e} \qquad Eq.S2$$

where R_e, A and d denote the electronic resistance, effective area, and specimen thickness, respectively.

Table S3 Ionic conductivity calculation of HG/PP and G/PP.

Specimen	R_b (Ω)	A (cm^2)	d (μm)	σ_{ion} (mS cm^{-1})
HG/PP	1.15	2.01	74	3.20
G/PP	1.91	2.01	68	1.77

*The ionic conductivity (σ_{ion}) of the specimen was calculated using the following equation:[13-15]

$$\sigma_{ion} = \frac{d}{AR_b} \qquad Eq.S3$$

where R_b, A and d denote the bulk resistance of the symmetric cell, effective area, and specimen thickness, respectively.

References:

1. M. Ali, M. Khan, F. Mahmood, C. F. M. Mbeugang, X. Xie, Y. Wang and B. Li, *Mater. Today Commun.*, 2025, **46**, 112743.
2. Q. Xia, K. Yan, K. Jin, Y. Wu, Y. Fu, D. Chen, H. Chen and H. Yue, *Chin. Chem. Lett.*, 2025, **36**, 110406.
3. L. Cheng, C. Ma, W. Lu, X. Wang, H. Yue, D. Zhang and Z. Xing, *Chem. Eng. J.*, 2022, **433**, 133527.
4. S. W. Cho, H. H. Choi, T. G. Senthamaraikannan, D. H. Lim, G. D. Park, C. Cho, S. M. Jeong, R. Saroha and J. S. Cho, *Chem. Eng. J.*, 2025, **512**, 162456.
5. K. Guo, X. Wang, J. Fan, Y. Min and Q. Xu, *Chem. Eng. J.*, 2022, **430**, 132705.
6. W. Sun, K. Guo, J. Fan, Y. Min and Q. Xu, *ACS Appl. Mater. Interfaces*, 2021, **13**, 16558-16566.
7. C. Y. Kwok, S. Xu, I. Kochetkov, L. Zhou and L. F. Nazar, *Energy Environ. Sci.*, 2023, **16**, 610-618.
8. S. Ohno and W. G. Zeier, *Acc. Mater. Res.*, 2021, **2**, 869-880.
9. K. Wang, T. Zhao, Y. Liu, T. Yu, G. Chen, W. Tang, L. Li, F. Wu and R. Chen, *Chem. Eng. J.*, 2024, **487**, 150300.
10. M. Qian, F. Wu, C. Yu, J. Zhang, T. Wang, J. Wang, T. Song and G. Tan, *Nano Energy*, 2024, **128**, 109841.
11. J. Kaspar, M. Graczyk-Zajac and R. Riedel, *Electrochim. Acta*, 2014, **115**, 665-670.
12. W. Wang, K. Xi, B. Li, H. Li, S. Liu, J. Wang, H. Zhao, H. Li, A. M. Abdelkader, X. Gao and G. Li, *Adv. Energy Mater.*, 2022, **12**, 2200160.
13. Y. Song, P. Tang, Y. Wang, L. Bi, Q. Liang, Y. Yao, Y. Qiu, L. He, Q. Xie, P. Dong, Y. Zhang, Y. Yao, J. Liao and S. Wang, *Small*, 2023, **19**, 2302386.
14. W. Lu, Y. Xu, C. Dazon, F. Macaulay, V. Pimenta and C. Serre, *Energy Mater.*, 2025, **5**, 500075.
15. S. Cao, T. Zhou, Y. Liu, W. Lu, A. Zhang, S. He, P. Yi, L. Ma, Z. Liu, F. Zuo, L. Cao, Z. Ren, M. Ye, H. Fang and J. Shen, *J. Am. Chem. Soc.*, 2025, **147**, 36626-36641.